Ultrafast single-shot diffraction imaging of nanoscale dynamics

ANTON BARTY[1,7]*, SÉBASTIEN BOUTET[2,3], MICHAEL J. BOGAN[1], STEFAN HAU-RIEGE[1], STEFANO MARCHESINI[1], KLAUS SOKOLOWSKI-TINTEN[4], NIKOLA STOJANOVIC[4], RA'ANAN TOBEY[5], HENRI EHRKE[5], ANDREA CAVALLERI[5,9], STEFAN DÜSTERER[6], MATTHIAS FRANK[1], SAŠA BAJT[1,8], BRUCE W. WOODS[1], M. MARVIN SEIBERT[3], JANOS HAJDU[3], ROLF TREUSCH[6] AND HENRY N. CHAPMAN[1,7,8]*

[1]Lawrence Livermore National Laboratory, 7000 East Avenue, Livermore, California 94550, USA
[2]Stanford Synchrotron Radiation Laboratory, Stanford Linear Accelerator Center, 2575 Sand Hill Road, Menlo Park, California 94025, USA
[3]Laboratory of Molecular Biophysics, Department of Cell and Molecular Biology, Uppsala University, Husargatan 3, Box 596, SE-75124 Uppsala, Sweden
[4]Institut für Experimentelle Physik, Universität Duisburg-Essen, Lotharstraße 1, 47048 Duisburg, Germany
[5]Department of Physics, Clarendon Laboratory, University of Oxford, Parks Road, Oxford OX1 3PU, UK
[6]Deutsches Elektronen-Synchrotron, DESY, Notkestraße 85, D-22607 Hamburg, Germany
[7]Center for Biophotonics Science and Technology, University of California, Davis, 2700 Stockton Boulevard, Ste 1400, Sacramento, California 95817, USA
[8]Centre for Free Electron Laser Science, Universität Hamburg at DESY, Notkestraße 85, 22607 Hamburg, Germany
[9]Max Planck Research Group for Structural Dynamics, Center for Free Electron Laser Science, Universität Hamburg at DESY, Notkestraße 85, 22607 Hamburg, Germany
*e-mail: a.barty@llnl.gov; henry.chapman@desy.de

Published online: 22 June 2008; doi:10.1038/nphoton.2008.128

The transient nanoscale dynamics of materials on femtosecond to picosecond timescales is of great interest in the study of condensed phase dynamics such as crack formation, phase separation and nucleation, and rapid fluctuations in the liquid state or in biologically relevant environments. The ability to take images in a single shot is the key to studying non-repetitive behaviour mechanisms, a capability that is of great importance in many of these problems. Using coherent diffraction imaging with femtosecond X-ray free-electron-laser pulses we capture time-series snapshots of a solid as it evolves on the ultrafast timescale. Artificial structures imprinted on a Si_3N_4 window are excited with an optical laser and undergo laser ablation, which is imaged with a spatial resolution of 50 nm and a temporal resolution of 10 ps. By using the shortest available free-electron-laser wavelengths[1] and proven synchronization methods[2] this technique could be extended to spatial resolutions of a few nanometres and temporal resolutions of a few tens of femtoseconds. This experiment opens the door to a new regime of time-resolved experiments in mesoscopic dynamics.

To date, optical pulses have made it possible to resolve dynamics on the femtosecond timescale, but the spatial resolution of these studies has been limited to a few micrometres[3]. On the other hand, femtosecond X-ray pulses have been used to detect Ångstrom-scale atomic motions in extended crystalline materials with long-range order through time-resolved diffraction experiments[4,5]. An entirely different methodology is needed to investigate the ultrafast dynamics of non-crystalline materials at nanometre length scales. Applications at these scales can be found in the study of fracture dynamics, shock formation, spallation, ablation, and plasma formation under extreme conditions. In the solid state it is desirable to directly image dynamic processes such as nucleation and phase growth, phase fluctuations and various forms of electronic or magnetic segregation.

Electron microscopes can provide nanometre to atomic resolution, and have recently been demonstrated with ultrafast pulses[6]. However, they have limited penetrating power and struggle to obtain high-quality single-shot images due to space-charge issues[7]. Synchrotron beams from third-generation sources have comparatively long pulse lengths of 10–100 ps, as determined by the shortest electron bunch length possible in a given storage ring. Synchrotron sources can produce short-pulse (~100 fs) X-rays when operated as femtosecond slicing sources[8], but produce comparatively weak X-ray beams of 1×10^7 photons per second. Along with X-ray pulses from femtosecond laser plasma sources[9,10] and high-harmonic-generation sources[11] this limits their use to non-destructive phenomena where weak signals can be accumulated over many repeatable excitations of the sample.

The intense femtosecond X-ray pulses from free-electron-laser (FEL) sources provide the penetrating power, spatial resolution and single-shot imaging capability necessary to probe transient phenomena at nanoscale length scales with femtosecond temporal resolution. With up to 1×10^{13} X-ray photons per pulse[1], sufficient photons can be scattered from an isolated nanoscale object to perform coherent X-ray diffraction imaging using a single femtosecond-duration X-ray pulse[12,13]. Here, we realize the ability to capture time-resolved snapshots of transient nanoscale dynamics by using ultrafast X-ray diffraction imaging and photon correlation spectroscopy techniques combined with an appropriate drive pulse. The 'shutter speed' of these measurements is

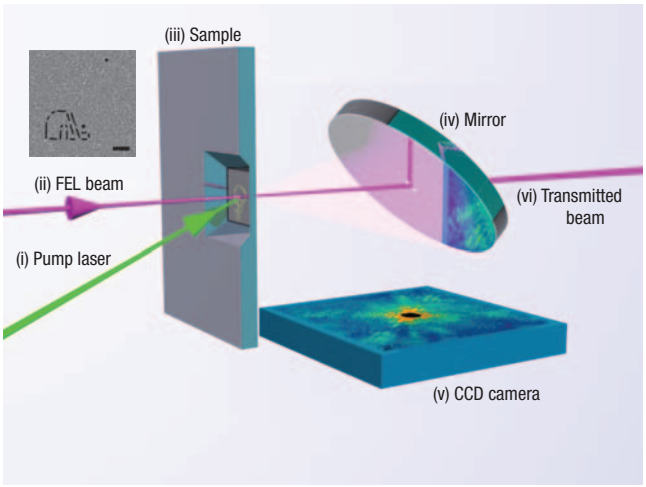

Figure 1 X-ray dynamic diffraction imaging. A visible-light laser beam (i) incident from the left is focused onto the sample (iii) and acts as the excitation pulse. A 10-fs duration soft X-ray pulse at a wavelength of 13.5 nm from the FEL (ii) is focused to a 20-μm spot in the same location as the visible-light laser at a continuously variable delay after the excitation pulse. The X-ray pulse diffracts from the sample, carrying information about the transient sample structure to the CCD detector (v) in the form of a coherent diffraction pattern. A 45° mirror (iv) is used to separate the direct beam from the diffracted light: the direct FEL beam (vi) passes straight through a hole in the mirror and is not detected in the CCD image. A 100-nm-thick zirconium filter over the CCD chip makes the detector blind to the laser excitation pulse. The sample (iii) consisted of a nanometre-resolution pattern etched into a silicon nitride membrane using a focused ion beam (FIB), providing a well-defined control sample so that the time evolution of a known structure could be observed. The path length from sample to CCD is 53 mm and the detected numerical aperture is 0.25, giving a spatial resolution of 27 nm in the sample plane.

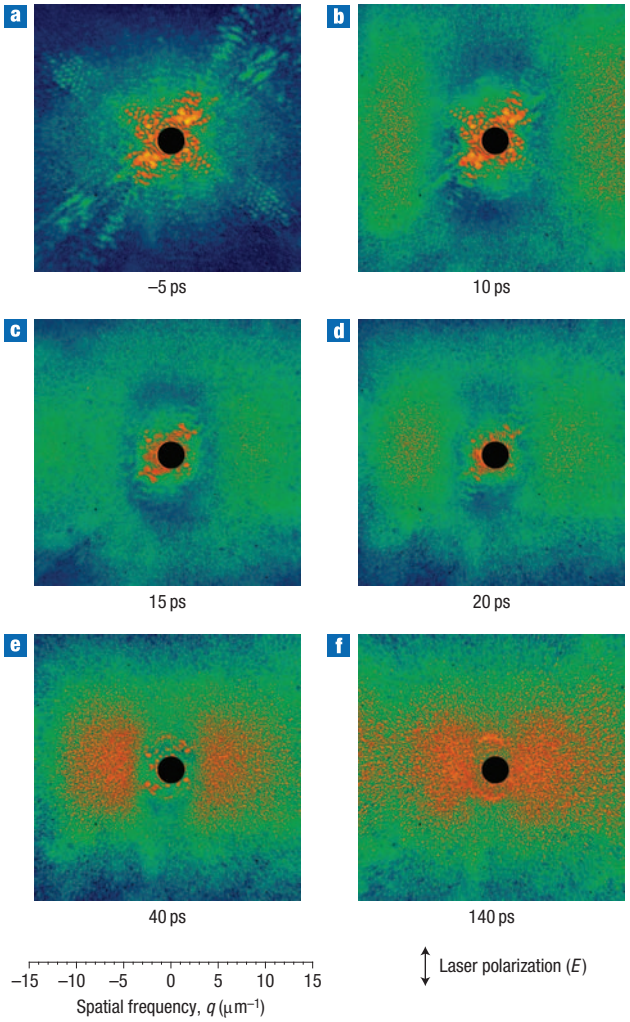

Figure 2 Sample evolution revealed by coherent X-ray diffraction. **a**–**f**, Measured single-shot diffraction patterns at −5 ps (**a**), corresponding to the object just before the laser excitation pulse, and diffraction patterns from the same object at 10 ps (**b**), 15 ps (**c**), 20 ps (**d**), 40 ps (**e**) and 140 ps (**f**) after the laser pulse. Gradual degradation of the nanofabricated sample is visible by the loss of high spatial frequency information in the diffraction patterns. The pump laser is p-polarized with the electric-field vector oriented vertically with respect to these images.

determined by the femtosecond duration of the FEL pulse, enabling us to obtain nanometre spatial resolution of violent and destructive events in which the sample is completely destroyed.

The experimental arrangement for dynamic diffraction imaging is shown in Fig. 1. Femtosecond X-ray pulses from the FLASH soft X-ray FEL facility at DESY in Hamburg, Germany, were used to probe sample evolution. FLASH was operated in single-bunch ultrashort-pulse mode, providing pulses close to transform limited and dominated by a single mode[14]. The pulses have almost complete transverse and longitudinal coherence, enabling almost the entire output to be used for coherent imaging. Each pulse consisted of a single 10-fs duration pulse of 13.5-nm soft X-rays focused to a ∼20-μm full-width at half-maximum (FWHM) spot on the sample using a 2 m focal length grazing incidence ellipsoidal mirror that forms a part of the BL2 beamline at FLASH. The mean energy of the X-ray pulses was 20 μJ, resulting in $\sim 1.4 \times 10^{12}$ X-ray photons per pulse. A fast photodiode sensitive to both visible and X-ray light provided relative pulse timing with subnanosecond resolution, and a long working distance microscope was used to ensure spatial overlap with the laser pump beam.

X-rays diffracted from the sample were detected on a soft X-ray charge-coupled device (CCD) camera. The angular acceptance of the CCD was 15° at the midpoint of the detector edges, corresponding to a numerical aperture of 0.25. This gives a diffraction-limited spatial resolution of 27 nm at the 13.5 nm soft X-ray wavelengths used in this experiment, where resolution is defined as the half-period of the finest horizontal and vertical spatial frequency in the image. The direct FEL beam was intense enough to destroy the CCD, and had to be separated from the comparatively weak diffracted light that comprised our measured signal. A 45° mirror with a graded multilayer coating reflected diffracted light onto the CCD camera, and the direct FEL beam passed straight through a hole in the mirror (see Methods).

For these experiments we used a nanofabricated test object as a well-defined control sample so that the evolution of a known structure could be observed. Nanometre resolution patterns were etched into a 20 nm thick silicon nitride membrane coated with a 100 nm thick iridium film supported in a silicon wafer window using a focused ion beam (FIB). A short-pulse linearly polarized laser (Nd:YLF operated at 523 nm) was used to initiate material ablation. The laser pulse length was 12.5 ps and delivered ∼25 μJ per pulse into a 30 μm FWHM focal spot on the sample, giving peak intensities of about 2.2×10^{11} W cm^{-2}. As

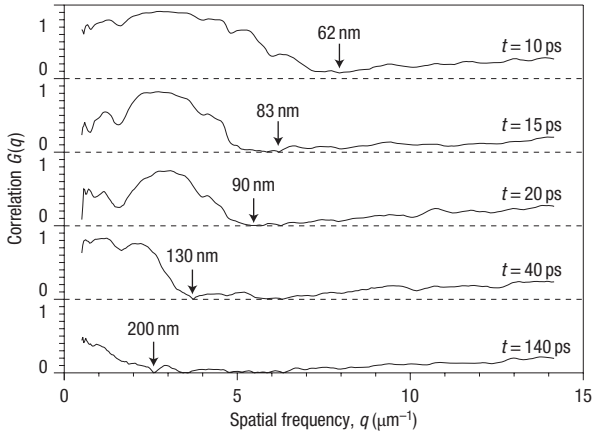

Figure 3 Correlation between diffraction patterns quantify the loss of mesoscale order. Resolution-dependent photon correlation spectra between the delayed diffraction patterns with the original object, showing the progressive loss of mesoscale order in the film structure information as a function of time. Arrows indicate the largest linewidth at which the correlation function first approaches zero, quantitatively estimating the length scale over which order is lost in the sample.

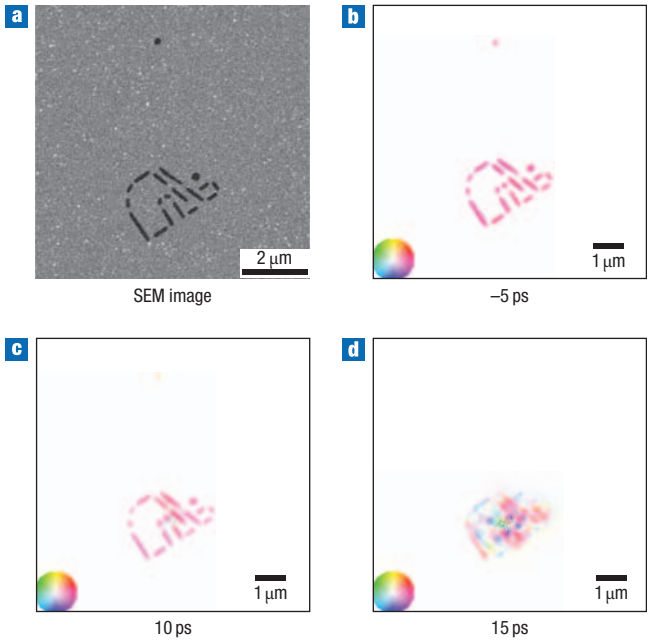

Figure 4 Reference object and objects retrieved using phase retrieval. **a**, Nanofabricated reference object. SEM is scanning electron microscopy. **b**–**d**, Images obtained using phase retrieval at various time delays after the laser excitation pulse: object before the laser excitation pulse (**b**), then at 10 ps delay (**c**) and 15 ps delay (**d**). Gradual degradation of the sample and loss of mesoscale order is visible, as is progressive disintegration of the object. The reconstructed complex-valued object is represented by hue and saturation (as indicated in the colour wheel).

the laser pulse energy was adequate to fully destroy the sample in a single pulse, separate identical copies of the sample were used to produce each individual time delay image. This laser was synchronized to the FEL photocathode laser with an optical delay line in the pump laser path for fine time delay control of the relative pulse timing.

A series of diffraction patterns revealing the time evolution of the sample when illuminated by the pump laser over the course of several picoseconds is shown in Fig. 2. Each time slice consists of an X-ray diffraction pattern acquired using the FEL probe pulse at different time delays after the laser excitation pulse. Immediately visible in the diffraction patterns is loss of information at high scattering angles, corresponding to loss of mesoscale order as the sample disintegrates. Additionally, structure is induced in the silicon nitride foil by the ablation pulse. The evolution of this structure gives rise to an increase in the intensity of fine speckles at frequencies, q, above about 5 μm^{-1}, primarily in the direction perpendicular to the pump laser polarization. Additionally a pair of strong diffraction peaks are clearly visible at ~140 ps delay, indicative of a light-induced periodic structure in the foil.[15] It can be seen from the patterns that speckle intensities increase at lower frequencies at later delays, corresponding to loss of high spatial frequency order in the sample as the physical structure on the membrane is destroyed over time.

Correlations between diffraction patterns at different time delays quantify the statistical properties of changes of mesoscale order. Known as X-ray photon correlation spectroscopy[16,17] (XPCS), a range of applications for this technique using FEL sources have recently been proposed[18]. Here, XPCS correlation functions comparing the diffraction pattern at $t = 0$ with subsequent diffraction patterns (Fig. 3), reveal the progressive disintegration and loss of mesoscale order in this sample as a function of time. Taking the point at which the normalized correlation function, $G(q)$, first approaches zero (arrows in Fig. 3), as the length scale over which the sample has disintegrated we observe the speed of the explosion initially propagating at between 5,000 and 6,000 m s^{-1} during the first 20 ps, slowing to 1,000–2,000 m s^{-1} by $t = 140$ ps as the resultant plasma expands and cools. Initial expansion speed is consistent with the speed of sound in the heated membrane, calculated to be 4,000–6,000 m s^{-1} (see Methods).

Applying phase retrieval techniques to the measured diffraction patterns yields images of the sample at each time step, enabling us to quantitatively visualize the structural degradation as a function of time. Each time slice consists of an X-ray diffraction pattern acquired using the FEL probe pulse (Fig. 2), to which iterative phase retrieval techniques[12,19] have been applied to obtain a real-space image of the object (Fig. 4; further details are in the Methods). The images in Fig. 4 confirm that the object has changed little in the first 10 ps, with the edges of the etched structure appearing only slightly blurred. However, by 15 ps, disintegration of the structure itself is clearly visible and only a portion of the pattern is recognizable.

Consider in particular the isolated pinhole structure shown in Fig. 4. The membrane was irradiated with 12.5 ps pulses at approximately 3 J cm^{-2}, a fluence well above the threshold for ablation in a free-standing film. Under the influence of the pump laser, surfaces will expand near the speed of sound. Given that both the lines and reference dot were manufactured to be ~130 nm wide, these lines should close up ~10–15 ps after the excitation pulse. This is consistent with what we see in the time evolution, where the reference dot can be seen to be half closed at $t = 10$ ps and no longer visible (corresponding to fully closed over) at $t = 15$ ps.

By combining the femtosecond temporal resolution of X-ray FELs with the nanoscale imaging capabilities of a coherent diffraction imaging geometry and a synchronous reaction trigger we have realized the ability to capture single-shot images of

nanoscale dynamics on the timescale of individual atomic motion. Single-shot dynamic diffraction imaging is unique in its ability to image non-repetitive phenomena where radiation-induced damage and intrinsic sample movement prevent the repeated accumulation of high-resolution scattering data using conventional X-ray sources. At the nanoscale, this technique has application to a wide range of dynamic phenomena, including the formation of dynamic inhomogeneities during chemical reactions, nucleation and phase segregation in the solid state, crack formation and spallation dynamics in solids, and potentially complex molecular rearrangements in biological cells. Looking further ahead, dynamic diffraction imaging can be readily extended to higher spatial resolution using the hard X-ray FELs currently under construction, in principle to near atomic resolution, and will ultimately enable the exploration of material dynamics at interatomic length scales on the timescale of atomic motion.

METHODS

Experiments were carried out at FLASH, the soft-X-ray FEL at DESY in Hamburg, using 13.5 nm light and an experimental geometry[12] and imaging apparatus[20] similar to that described elsewhere.

Samples consisted of a pattern cut into a silicon nitride membrane with a dual-beam FIB instrument (FEI, National Center for Electron Microscopy, Lawrence Berkeley National Laboratory), using a 100 pA beam of 30 keV Ga^+ ions. Sample substrates consisted of a free-standing 20 nm thick low-stress silicon nitride membrane film coated with a 100 nm thick iridium film. Membranes were supported by 100 μm square etched openings or windows in a silicon wafer frame, and were manufactured at the Microfabrication Center at the Lawrence Livermore National Laboratory.

The ablation pulse was provided by a 523 nm pulsed Nd:YLF laser provided by the FLASH facility. This laser is essentially a copy of the photocathode laser producing the electron pulses for the FEL and can thus provide the same pulse pattern as the FEL[21]. The actively mode-locked oscillator of the laser system allows a synchronization better than 1 ps jitter to the XUV pulses of the FEL[22]. This laser was focused to an approximately 30 μm FWHM spot on the sample and delivered approximately 25 μJ per pulse, producing fluences on the sample of between 2 and 6 J cm^{-2}. The pulse length for the pump laser was 12.5 ps, giving peak intensities of about 2.2×10^{11} W cm^{-2} on the sample, adequate to fully destroy the sample in a single pulse. The finite duration of the excitation pulse used in these experiments leads to a systematic uncertainty of ~2.5 ps in the relative pump-probe pulse timing.

Correlations between different diffraction patterns were quantified by evaluating the normalized correlation function

$$G(q) = \frac{I_1'(q) \cdot I_2'(q)}{\|I_1'(q)\| \ \|I_2'(q)\|} \quad (1)$$

as a function of spatial frequency q, where the vectors $I_1(q)$ and $I_2(q)$ have first been adjusted to have zero mean,

$$I_n' = I_n(q) - \langle I_n(q) \rangle \quad (2)$$

and $\langle \cdots \rangle$ is the average over vector elements. For this analysis, the vectors $I_1(q)$ and $I_2(q)$ consisted of the measured intensities within an annulus 20 pixels wide centred with respect to the diffraction pattern and stepped across the diffraction pattern in steps of one pixel to produce the plot shown in Fig. 3. This correlation function returns a value between 0 and 1 depending on the degree of correlation between the two vectors $I_1(q)$ and $I_2(q)$, with a perfectly correlated set of data yields $G(q) = 1$ for all values of q.

As a result of finite photon counts and some non-reproducibility present during the FIB milling used to produce the samples, perfect correlation between two exposures at identical delays is not expected. Comparison of the $t = 0$ diffraction pattern with an image captured without the drive laser (diffraction pattern not shown) revealed a good correlation out to the edge of the CCD camera.

The damage-dynamics timescale is related to the velocity of sound of the material, which, in turn, depends on the energy density. Because of uncertainties in the temperature dependence of the optical properties of iridium at a wavelength of 523 nm, we can only estimate an upper limit for the deposited energy density assuming full absorption. The iridium and Si_3N_4 film equilibrate within a few picoseconds or less[23], so we can use the equilibrium QEOS (quotidian equation-of-state) model[24] to find the temperature and sound velocity of the material. An upper limit for the temperature is 4×10^4 K, corresponding to an initial sound velocity of 6.3×10^3 m s^{-1} at solid density. At room temperature, the sound velocity of iridium is 4.0×10^3 m s^{-1}. Uncertainties in the deposited energy could be reduced by appropriate metrology to measure the incoming, reflected and transmitted laser fluences and uncertainties in the measured expansion velocity arise primarily from variation in the laser timing. Both uncertainties could be reduced in future experiments. After the initial laser pulse, the plasma will expand and cool, consistent with the observed decrease in expansion velocity.

Image reconstruction was carried out using iterative transform phase retrieval techniques. Here, we used the RAAR algorithm[25,26] coupled with the Shrinkwrap dynamic support refinement algorithm[19], although a range of alternative phase retrieval schemes could no doubt be used[27–30]. The object is allowed to be complex-valued to take into account phase aberrations in the illuminating beam and complex object structure at later time steps. Initial support was based on thresholding the object autocorrelation at $t = 0$ then allowed to evolve dynamically. The support constraint was calculated every 100 iterations by selecting pixels with intensity values greater than 5% of the maximum image intensity, after first blurring the image with a gaussian kernel. The blurring kernel was initially set to 3 pixels FWHM and was gradually reduced to 1 pixel FWHM by iteration 1,500. The final solution was the sum of 1,000 separate iterates, enabling fluctuations in recovered phase to average into a final solution. Summation commenced at iteration 2,000 with the support fixed (that is, no longer evolving) and every third iterate summed through to iteration 5,000. Unconstrained modes contained in both the support and beamstop regions were not adequately constrained during phase retrieval and were filtered out of the final solution[31]. We found that phase retrieval became progressively more difficult as the delay increased, correlating with loss of detailed structure in the sample. To assist in image reconstruction the solution and support obtained for $t = 0$ was used as an initial guess for phase retrieval at longer time delays, then allowed to evolve into the solution for the delayed ($t > 0$) diffraction pattern using the same algorithm and procedures described above.

Received 13 February 2008; accepted 23 May 2008; published 22 June 2008.

References

1. Ackerman, W. *et al.* Operation of a free-electron laser from the extreme ultraviolet to the water window. *Nature Photonics* **1,** 336–342 (2007).
2. Cavalieri, A. L. *et al.* Clocking femtosecond X rays. *Phys. Rev. Lett* **94,** 114801 (2005).
3. Sokolowski-Tinten, K. *et al.* Transients states of matter during short pulse laser ablation. *Phys. Rev. Lett.* **81,** 224–227 (1998).
4. Siders, C. W. *et al.* Direct measurement of non-thermal melting using ultrafast X-ray diffraction. *Science* **286,** 1340–1342 (1999).
5. Sokolowski-Tinten, K. *et al.* Femtosecond X-ray measurement of coherent lattice vibrations near the Lindemann stability limit. *Nature* **422,** 287–289 (2003).
6. Lobastov, V. A., Srinivasan, R. & Zewail, A. H. Four-dimensional ultrafast electron microscopy. *Proc. Natl Acad. Sci. USA* **102,** 7069–7073 (2005).
7. Armstrong, M. R. *et al.* Practical considerations for high spatial and temporal resolution dynamic transmission electron microscopy. *Ultramicroscopy* **107,** 356–367 (2007)
8. Schoenlein, R. W. *et al.* Generation of femtosecond pulses of synchrotron radiation. *Science* **287,** 2237–2240 (2000)
9. Rischel, C. *et al.* Femtosecond time-resolved X-ray diffraction from laser-heated organic films. *Nature* **390,** 490–492 (1997).
10. Rose-Petruck, C. *et al.* Picosecond milliångström lattice dynamics measured by ultrafast X-ray diffraction. *Nature* **398,** 310–312 (1999).
11. Bartels, R. A. *et al.* Generation of spatially coherent light at extreme ultraviolet wavelengths. *Science* **297,** 376–378 (2002)
12. Chapman, H. N. *et al.* Femtosecond diffractive imaging with a soft-X-ray free-electron laser. *Nature Physics* **2,** 839–843 (2006)
13. Chapman, H. N. *et al.* Femtosecond time-delay X-ray holography. *Nature* **448,** 676–679 (2007).
14. Ischebeck, I. *et al.* Study of the transverse coherence at the TTF free electron laser. *Nucl. Instrum. Meth. A* **507,** 175–180 (2003).
15. Young, J. F., Preston, J. S., van Driel, H. M. & Sipe, J. E. Laser-induced periodic surface structure. II. Experiments on Ge, Si, Al, and brass. *Phys. Rev. B* **27,** 1155–1172 (1983).
16. Brauer, S. *et al.* X-ray intensity fluctuation spectroscopy observations of critical dynamics in Fe_3Al. *Phys. Rev. Lett.* **74,** 2010–2013 (1995).
17. Dierker, S. B., Pindak, S. R., Fleming, R., Robinson, I. & Berman, L. X-ray photon correlation spectroscopy study of Brownian motion if gold colloids in glycerol. *Phys. Rev. Lett.* **75,** 449–452 (1995).
18. Gŕubel, G., Stephenson, G. B., Gutt, C., Sinn, H. & Tschentscher, T. XPCS at the European X-ray free electron laser facility. *Nucl. Instrum. Meth. B* **267,** 357–367 (2007).
19. Marchesini, S. *et al.* X-ray image reconstruction from a diffraction pattern alone. *Phys. Rev. B* **68,** 140101 (2003).
20. Bajt, S. *et al.* A camera for coherent diffractive imaging and holography with a soft-X-ray free electron laser. *Appl. Opt.* **47,** 1673–1683 (2008).

21. Will, I., Koss, G. & Templin, I. The upgraded photocathode laser of the TESLA test facility. *Nucl. Instrum. Meth. A* **541,** 467–477 (2005).
22. Radcliffe, P. *et al.* An experiment for two-color photoionization using high intensity extreme-UV free electron and near-IR laser pulses. *Nucl. Instrum. Meth. A* **583,** 516–525 (2007).
23. Hau-Riege, S. P., London, R. A., Chapman, H. N. & Bergh, M. Soft-x-ray free-electron-laser interaction with materials. *Phys Rev E* **76,** 046403 (2007).
24. More, R. M., Warren, K. H., Young, D. A. & Zimmerman, G. B. A new quotidian equation of state (QEOS) for hot dense matter. *Phys. Fluids* **31,** 3059–3078 (1988).
25. Chapman, H. N. *et al.* High-resolution ab initio three-dimensional X-ray diffraction microscopy. *J. Opt. Soc. Am. A* **23,** 1179–1200 (2006).
26. Luke, D. R., Relaxed averaged alternating reflections for diffraction imaging. *Inverse Problems* **21,** 37–50 (2005).
27. Fienup, J. R. Reconstruction of an object from the modulus of its Fourier transform. *Opt. Lett.* **3,** 27–29 (1978).
28. Miao, J., Charalambous, P., Kirz, J. & Sayre, D. Extending the methodology of X-ray crystallography to allow imaging of micrometre-sized non-crystalline specimens. *Nature* **400,** 342–344 (1999).
29. Elser, V. Phase retrieval by iterated projections *J. Opt. Soc. Am. A* **20,** 40–55 (2003).
30. Hau-Riege, S. P. *et al.* SPEDEN: reconstructing single particles from their diffraction patterns. *Acta. Cryst. A* **60,** 294–305 (2004).
31. Shapiro, D. *et al.* Biological imaging by soft X-ray diffraction microscopy. *Proc. Natl Acad. Sci.* USA **102,** 15343 (2005).

Acknowledgements

Special thanks are given to the scientific and technical staff of FLASH at DESY, Hamburg, in particular to T. Tschentscher, J. Schneider, J. Feldhaus, R.L. Johnson, U. Hahn, T. Nünez, K. Tiedtke, H. Redlin, S. Toleikis, E.L. Saldin, E.A. Schneidmiller and M.V. Yurkov. We also thank J. Alameda, E. Spiller, E. Gullikson, A. Aquila, F. Dollar, T. McCarville, F. Weber, J. Crawford, C. Stockton, M. Haro, J. Robinson, H. Thomas and E. Eremina for technical help with these experiments. This work was supported by the following agencies: The US Department of Energy (DOE) Lawrence Livermore National Laboratory; The National Science Foundation Center for Biophotonics, University of California, Davis; The Advanced Light Source and National Centre for Electron Microscopy, Lawrence Berkeley Laboratory, under contract DE-AC03-76SF00098; Natural Sciences and Engineering Research Council of Canada (NSERC Postdoctoral Fellowship to M.J.B.); Sven and Lilly Lawskis Foundation (doctoral fellowship to M.M.S.); the US Department of Energy Office of Science to the Stanford Linear Accelerator Center; the European Union (TUIXS); the German Federal Ministry of Education and Research (FSP 301); The Swedish Research Council; The Swedish Foundation for International Cooperation in Research and Higher Education; and The Swedish Foundation for Strategic Research. This work was performed under the auspices of the US DOE by Lawrence Livermore National Laboratory in part under contract W-7405-Eng-48 and in part under contract DE-AC52- 07NA27344.

Author contributions

H.N.C., A.B., S.Boutet and K.S.T. conceived the experiment, and A.B., H.N.C., S.Boutet, M.J.B., S.M., B.W.W., M.F. and S.Bajt contributed to its design. Samples were prepared by S.Boutet, M.J.B. and S.Bajt. A.B., S.Boutet, M.J.B., S.M., K.S.T., N.S., R.T., H.E., A.C., S.D., M.F., B.W.W., M.M.S., R.T., and J.H. carried out the experiment, in addition to K.S.T., N.S., R.T., H.E., A.C. and S.D., who were responsible for the ablation laser pulse and synchronization. A.B., H.N.C., S.M. and K.S.T. analysed the data. S.P.H.R. performed hydrodynamic modelling of sample ablation. All authors discussed the results and contributed to the final manuscript.

Author information

Reprints and permission information is available online at http://npg.nature.com/reprintsandpermissions/. Correspondence and requests for materials should be addressed to A.B. and H.N.C.